IDENTIFICATION AND DETECTION OF BACTERIAL SPORES WITH A PASSIVE FTIR IN AN OPEN AIR POINT RELEASE

Avishai Ben-David, Francis M. D'Amico, Hsuan Ren, Darren K. Emge, Alan C. Samuels, James O. Jensen and William R. Loerop

Science and Technology Corporation, 500 Edgewood Road, Suite 205, Edgewood, Maryland 21040. E-mail: avishai.bendavid@apgea.army.mil, Tel: 410-436-6631

U.S. Army Edgewood Chemical Biological Center, Aberdeen Proving Ground, MD 21010-5424

ABSTRACT

A simple experiment was conducted in order to test the feasibility of a high-sensitivity Fourier transform infrared (FTIR) spectrometer a passive infrared spectrometer to measure open-air point release of dry *Bacillus subtilis* var. *niger* (BG) spores. The release was partially contained in order to provide a stable cloud. Measurements were taken continuously through a horizontal line of sight with a complex background (sky and mountains at a distance of a few tens of kilometers) at a distance of 50 meters. The temperature difference (background to ambient air) was a few degrees Kelvin. Advanced identification and detection algorithms, based on radiative transfer theory and statistical signal processing methods were developed and used during the experiment. The deduced absorption spectra (Identification) show an excellent match to a BG absorption spectrum and thus indicate that the released material was BG. Analysis of the time sequence of the measurements via an adaptive detection threshold coincides very well (Detection) with the presence of the BG during the measurements. For completion we also show measurements of Kaolin dust where the ability to distinguish between the spectrum of BG and Kaolin is shown. Our experiment and analysis clearly show the feasibility of passive remote sensors to detect and identify BG particles. These results are encouraging and more experiments to validate our models and to explore their limitations are planned.

INTRODUCTION

In the last decade there has been a great interest in the possibility of identification and detection of bacterial spores with a passive Fourier transform infrared (FTIR) spectrometer in an open-air environment. Many in the scientific community doubted that possibility due to lack of sensor's required sensitivity and the overwhelmed problem of background thermal radiance (ambient atmosphere) that is superimposed on a faint thermal emission (or absorption) by the bacterial spores. In this work we show successful results of a recent experiment where we measured an open-air release of dry *Bacillus subtilis* var. *niger* (BG) spores and Kaolin dust with a high-sensitivity FTIR sensor and used advanced identification detection and estimation algorithms to analyze the measurements. We show the deduced spectrum of Kaolin dust in order to demonstrate our ability to distinguish between BG and Kaolin.

RADIATIVE TRANSFER MODEL

We consider a simple geometry (Fig. 1) for homogeneous atmosphere at temperature T where the sensor line of sight (LOS) is nearly horizontal; pointing at a topographic target at a far distance, or pointing to infinity (when no topographic target is present at the end of LOS). A cloud of size L (m) containing aerosols (or vapor of interest) is at a distance z from the sensor and atmospheric layer is present between the cloud and the topographic target. The

Report Documentation Page

Form Approved
OMB No. 0704-0188

1. REPORT DATE	2. REPORT TYPE	3. DATES COVERED
01 JUL 2003	**N/A**	**-**

4. TITLE AND SUBTITLE	5a. CONTRACT NUMBER
Identification And Detection Of Bacterial Spores With A Passive FTIR In An Open Air Point Release	5b. GRANT NUMBER
	5c. PROGRAM ELEMENT NUMBER
6. AUTHOR(S)	5d. PROJECT NUMBER
	5e. TASK NUMBER
	5f. WORK UNIT NUMBER
7. PERFORMING ORGANIZATION NAME(S) AND ADDRESS(ES) **Science and Technology Corporation, 500 Edgewood Road, Suite 205, Edgewood, Maryland 21040**	8. PERFORMING ORGANIZATION REPORT NUMBER
9. SPONSORING/MONITORING AGENCY NAME(S) AND ADDRESS(ES)	10. SPONSOR/MONITOR'S ACRONYM(S)
	11. SPONSOR/MONITOR'S REPORT NUMBER(S)

12. DISTRIBUTION/AVAILABILITY STATEMENT
Approved for public release, distribution unlimited

13. SUPPLEMENTARY NOTES
See also ADM001523., The original document contains color images.

14. ABSTRACT

15. SUBJECT TERMS

16. SECURITY CLASSIFICATION OF:			17. LIMITATION OF ABSTRACT	18. NUMBER OF PAGES	19a. NAME OF RESPONSIBLE PERSON
a. REPORT	b. ABSTRACT	c. THIS PAGE			
unclassified	**unclassified**	**unclassified**	**UU**	**21**	

aerosol cloud (or vapor) are at temperature T_c with mass-column-density ρ ($g\,m^{-2}$), $\rho = CL$ where C is mass concentration ($g\,m^{-3}$) and α ($m^2\ g^{-1}$) is mass extinction coefficient.

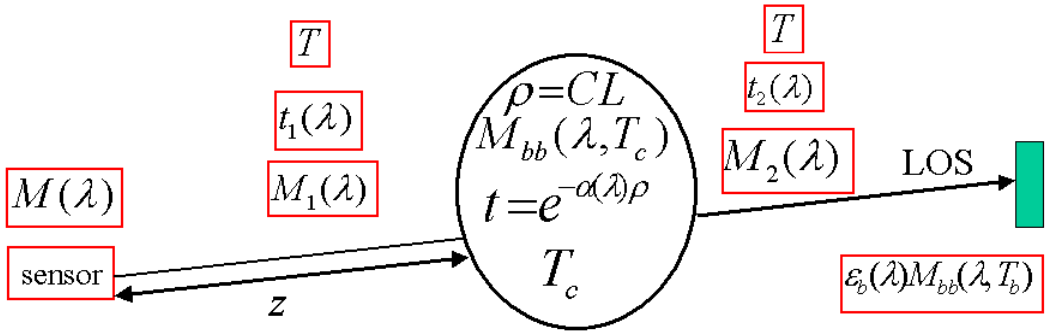

Figure 1. A simplified geometry for sensor measurements of a cloud at a distance z.

M_1 is the atmospheric radiance between the cloud and the sensor ; $e^{-\alpha(\lambda)\rho}$ is the cloud transmission ; $M_{bb}(T)$ is the Planck function describing the radiance of a blackbody at temperature T ; t_1 is the atmospheric transmission between the cloud and the sensor ; M_2 and t_2 are the atmospheric radiance and transmission between the cloud and the end of LOS ; $M_{bb}(T_b)$ is the Planck function of the topographic target with temperature T_b and emissivity.

In Figure 2 we show the atmospheric radiances M_1, M_2 and the transmissions t_1, t_2 for a distance z of 1, 3 and 5 km computed with the MODTRAN atmospheric radiative transfer code[1] for a standard desert atmosphere with visibility of 23 km, ground albedo of 0.2 and a line of sight 1^o above the horizon.

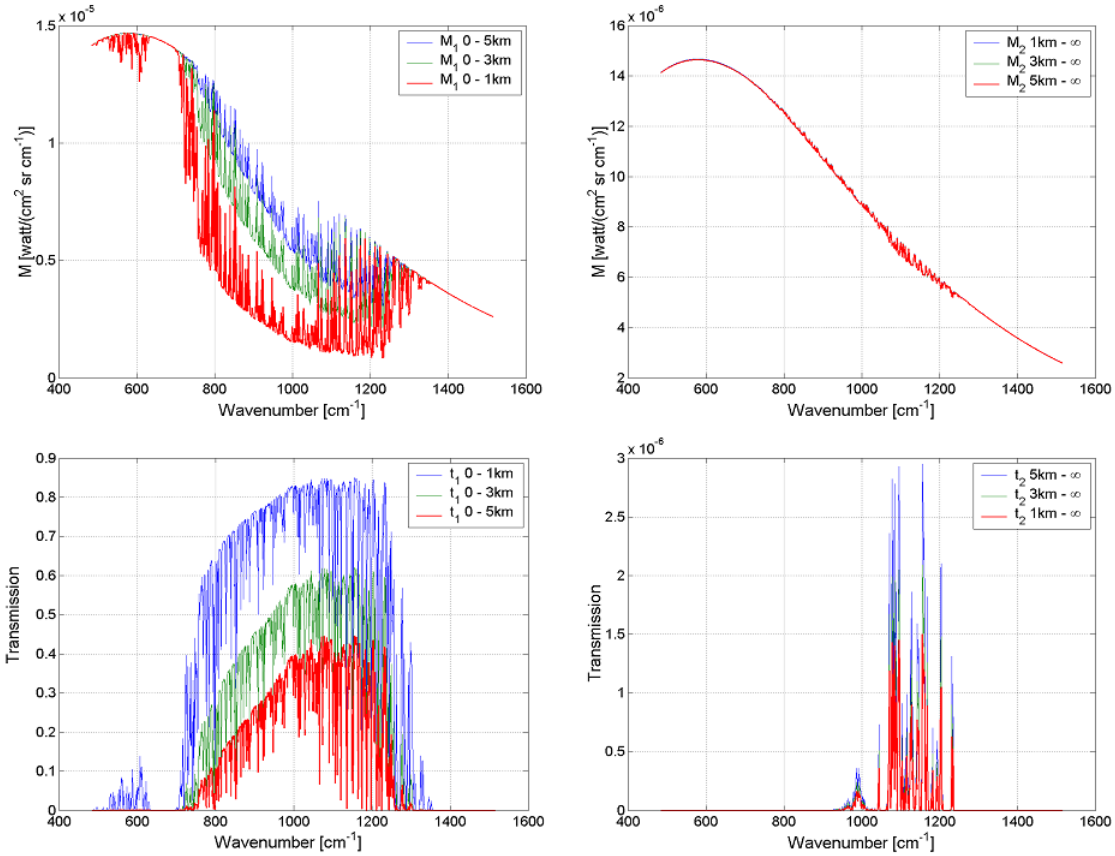

Figure 2. Atmospheric radiances M_1, M_2 and transmissions t_1, t_2 for a distance z of 1, 3 and 5 km (legend is in the same order as the curves).

We can separate the sensor measurements into two parts; signal-information that is affected by the presence of the cloud via its transmission $e^{-\alpha(\lambda)\rho}$ and a second part that is not affected by the presence of the cloud and can be viewed as an offset. In Figure 3, we show the mass extinction coefficient for BG material and in Figures 4 through 6, we show the signal-information and the sensor radiance $M(\lambda)$ for three scenarios where the LOS is 1 degree above the horizon pointing to infinity (i.e., no topographical target at the end of LOS) and a cloud of 100 m with BG bio-aerosols is within the LOS.

Figures 4 through 6 demonstrate the enormous difficulty of detecting BG bio-aerosols with passive FTIR sensor. For the bio-aerosols we use a log-normal size distribution with mean diameter $\mu = \ln(1.74\mu m)$ and standard deviation of $\sigma = \ln(2.09\mu m)$ where 99% of the aerosols are with diameter less than $10\mu m$, and the total mass for aerosol number density $N = 1\, cm^{-3}$ is $4 \cdot 10^{-11}\, g$.

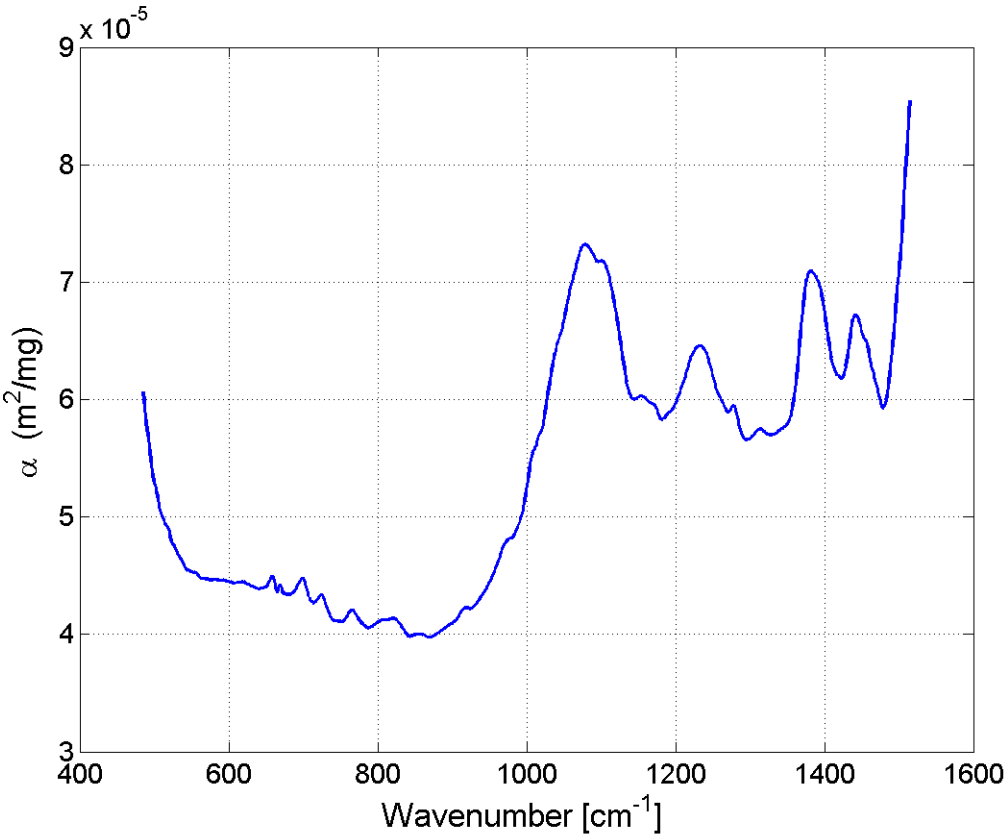

Fig. 3 – Mass extinction coefficient of BG material

In Fig. 4 we use an isothermal atmosphere (i.e., a blackbody at temperature T) where the cloud is at $R = 0\,km$ (t_1=1) and is 5 ^{o}K colder than the atmosphere. This case is an ideal case and even for this case we see that only for a high aerosol concentration of 4000 $mg\ m^{-2}$ (equivalent to particle number density N=10^3 particles per cm^{-3}) one can see some spectral features in the signal-information (right y-axis) portion of the measurements whose magnitude is about one order of magnitude lower than the total signal (left y-axis).

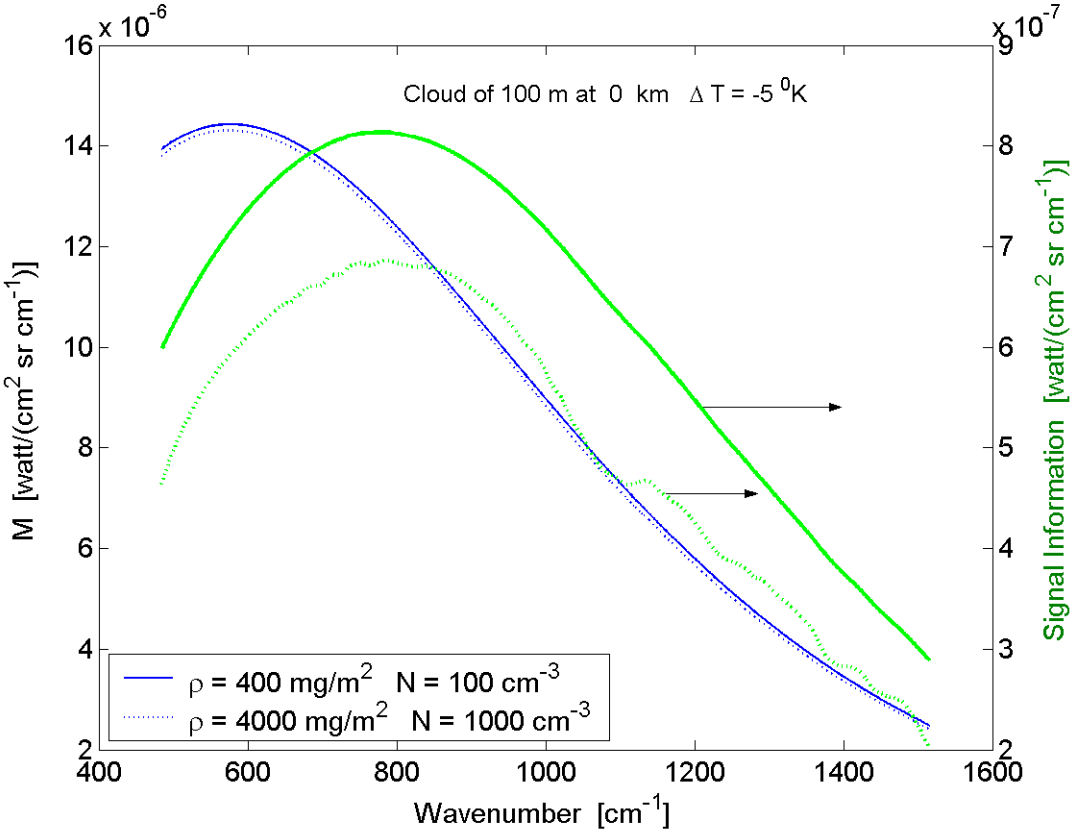

Figure 4. Simulated measurements M (left y-axis) and the signal information portion (right y-axis) that contain information on the cloud for bio-aerosol cloud of size 100 m containing *N* particles per cm^3. The bio-aerosol particles are at 5 ^{0}K colder than the ambient atmosphere. The atmosphere is an isothermal atmosphere (ideal case) represented by a blackbody at temperature *T*. The sensor LOS is horizontal pointing to infinity. Dotted lines (green and blue) are for $N = 1000\ cm^{-3}$ and solid lines are for $N = 100\ cm^{-3}$.

In Figure 5, we replace the isothermal blackbody atmosphere with a MODTRAN simulated atmosphere. This case represents a simple scenario. In this figure we see that the signal-information part contains many atmospheric spectral features and it is practically impossible to see the spectral features of the bio-aerosol (Fig. 3). Note that the signal-information part is one order of magnitude lower than the total signal.

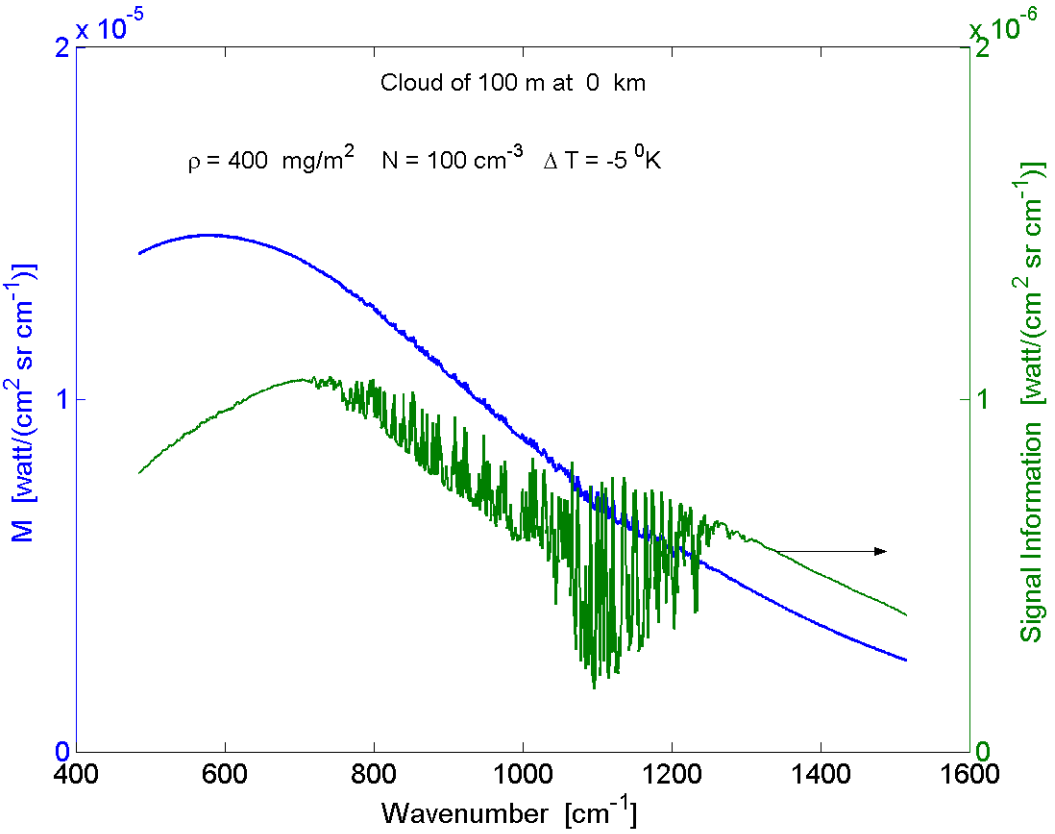

Figure 5. Same as Figure 4 but the atmosphere is simulated by MODTRAN radiative transfer program.

Figure 6 is the same as Figure 5 but the cloud is moved to a distance of 1 km from the sensor and thus we introduce atmospheric transmission and thermal radiation between the sensor and the cloud. This scenario represents a complex case.

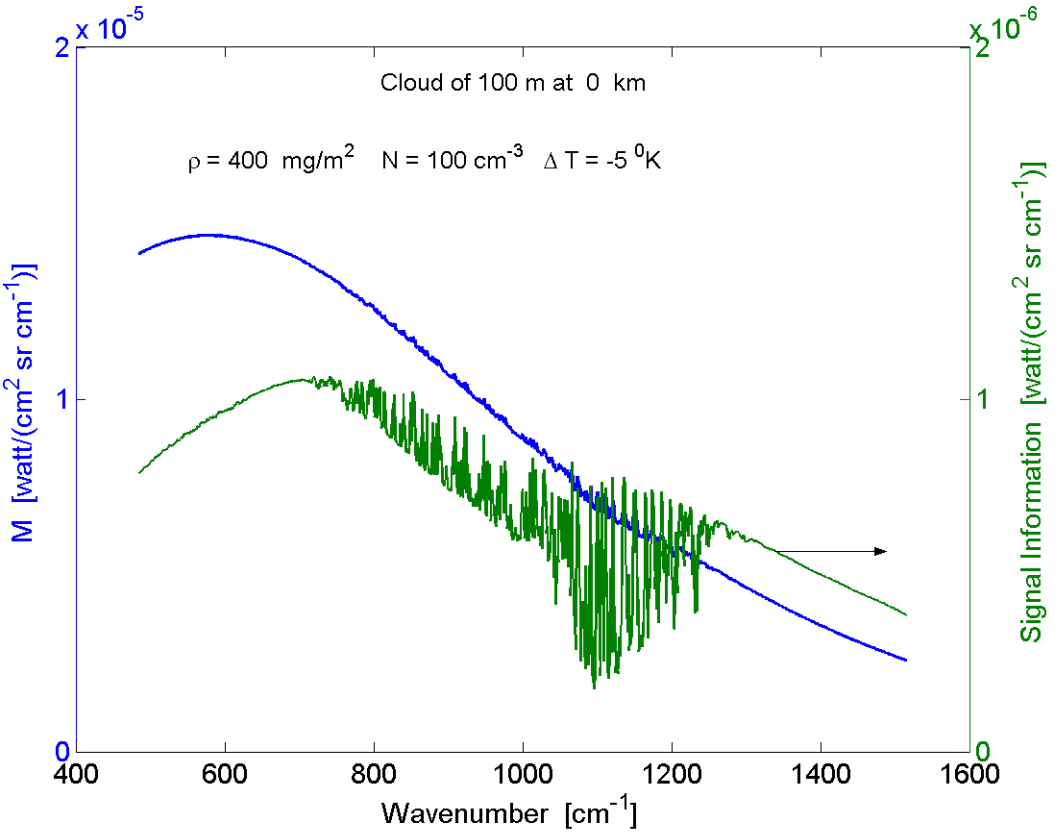

Figure 6. Same as Fig. 5 but the cloud is at 1 km from the sensor.

ALGORITHMS

We address two problems: (a) identification (deducing $\alpha(\lambda)$) of the aerosols along the LOS and (b) estimation of the mass-column density ρ in the measurements or the detection of the presence of aerosols in the measurements. The detection objective contrary to estimation is a measure of a change (anomaly) with respect to a reference (background) measurement – a change that indicates the presence of the aerosol cloud in the LOS.

1. IDENTIFICATION

We develop an identification algorithm where we deduce the extinction spectrum $\hat{\alpha}(\lambda, n)$ for each of the n sensor measurements $M(\lambda, n)$. If the expected value ($E[\bullet]$ denotes an expectation process) $\hat{\alpha}(\lambda) = E[\hat{\alpha}(\lambda, n)]$ of the n deduced spectra is highly correlated with the library spectrum $\alpha(\lambda)$ of the aerosols (or vapor) in the LOS we "declare" that identification was made.

2. DETECTION

The objective of the detection algorithm is to estimate the mass-column concentration $\rho(n)$ for each of the n sensor measurements $M(\lambda, n)$, and to set a threshold of detection γ such that for $\rho(n) > \gamma$ we declare that the cloud was present in the LOS. We present two types of detection algorithms. The first algorithm estimates the mass-column-density

$\rho(n)$ and set a threshold for detection γ. The second algorithm is a matched filter that produce a detection score $s(n)$ and set a threshold for detection γ such that for $s(n) > \gamma$ we declare a detection.

Assume that we have a set of measurements $M_0(\lambda, n_0)$ that are believed to represent n_0 possible realizations of background conditions for the absence of aerosol-cloud. For each of the possible realizations we estimate the mass-column-density $\rho(n \mid n_0)$ for any of the n measurements. The solution $\rho(n)$ is given by performing an expectation on all the possible n_0 solutions $\hat{\rho}(n) = E[\hat{\rho}(n \mid n_0)]$.

For detection of the presence of aerosol-cloud it is very useful to be able to set a threshold of detection γ that will divide $\hat{\rho}(n)$ into two distinct classes; target-signal (aerosol-cloud in our case) is present or target-signal is absent. Detection models are based on constructing a test statistic derived from the probability density function (pdf) of the data ($\rho(n)$ in our case), which is contaminated with noise. The noise may consist of random noise and interference (structured noise) from "look alike" targets that are unwanted and obscure the desired target signature. The objective of the test statistic is to decide between two hypotheses, H_0 and H_1 regarding the data. For the null hypothesis H_0 the interpretation is that the data does not contain the target-signal of interest and consists of only noise and interference. The alternative hypothesis H_1 is that the data does contain the target-signal in addition to noise and interference. A pdf model for the two hypothesizes enables us to compute probabilities of detection and false alarm and to set a threshold for detection under the constraint of maintaining a constant probability of false alarm rate. We estimate the parameters of the pdf model with an Expectation–Maximization (EM) algorithm and compute the threshold γ. The threshold γ minimizes the sum of the probability of false alarm (i.e., deciding H_1 when H_0 is true) and the probability of a miss (i.e., deciding H_0 when H_1 is true).

We use the classical matched filter algorithm where a detector score $s(n)$ is computed from $M(\lambda, n)$. A high detection score indicates that the target-signal is present. The matched filter is based on a whitening process of the spectral content of the measurements under the H_0 hypothesis. Any signal $M(\lambda, n)$ that is outside the whitened sphere in the spectral direction of $\alpha(\lambda)$ is an anomaly declared to be a target-signal measured under the H_1 hypothesis (i.e., detection).

EXPERIMENTS

Two experiments were conducted at Dugway Proving Ground, Utah on July 17, 2002 with a high-sensitivity Fourier transform infrared (FTIR) spectrometer[2] (HISPEC) which is a classical Michelson interferometer. The noise equivalent spectral radiance of the sensor is $1-2\cdot 10^{-9}$ $watt/(cm^2\, sr\, cm^{-1})$ and the wavelength resolution is 3.85 cm^{-1}. A detailed explanation of the FTIR spectrometer specifications and its design are given by Schildkraut, Connors and Ben-David[2]. The FTIR interferogram measurements were converted to spectral measurements[3] . In the first experiment an open-air release of dry BG spores was conducted. In the second experiment an open-air release of Kaolin dust was conducted.

A rectangular box with two open faces ($3\ m \times 3\ m$) and length of $6\ m$, in a shape of a tunnel was placed 50 *m* from the sensor. Aerosol cloud (BG or Kaolin) was generated within the box (54 m^3) with a small dust blower and was carried by the wind along the length of the box,

away from the sensor. Aerosols were continuously injected into the open chamber (box) with the dust blower that acted as a point-source release. A cloud (with very uneven density) was sustained in the chamber during the measurements that were taken through a horizontal line of sight with a complex background (sky and mountains at a distance of a few tens of kilometers) at the end of the LOS. A strong wind and cloudy sky persisted during the measurements and at times very light rain occurred. The sensor's footprint at the chamber distance (0.5 degrees FOV) can be taken as a cylinder (0.83 m^3) with diameter of 0.42 *m* and 6 *m* length. The LOS was approximately in the direction of the wind.

1. OPEN-AIR RELEASE OF DRY BG AEROSOLS

A total of 158 *g* of dry BG spores was used during the first experiment (an average of 120 *mg* per measurement). An estimate of the mass-column-density during the release ranges between a minimum of $\rho_{\min} = \frac{120}{54} \times 6 = 13 \ mg \ m^{-2}$ assuming that the total volume of the chamber was filled to a maximum of $\rho_{\max} = \frac{120}{0.83} \times 6 = 870 \ mg \ m^{-2}$ assuming that all the 120 *mg* bio-aerosols are within the sensor's FOV. For the assumed lognormal size distribution of the BG particles the minimum and maximum number density of the BG particles are 54 cm^{-3} and 3600 cm^{-3} respectively.

In Fig. 7 we show an estimate of the spectral brightness temperature difference between the ambient atmospheric temperature (deduced at wavelengths regions around 1400 cm^{-1}) and the effective brightness temperature along the LOS. The bio-aerosols spectral extinction coefficient is superimposed in the figure to show that in most wavenumber regions $\Delta T(\lambda)$ is less than 5 ^{o}K. For $\Delta T(\lambda)$=0 a thermo-dynamical equilibrium exists and if we neglect scattering and consider only absorption and emission mechanisms then no spectral information is available on the bio-aerosols (e.g., the secondary peak at 1380 cm^{-1} can not be resolved).

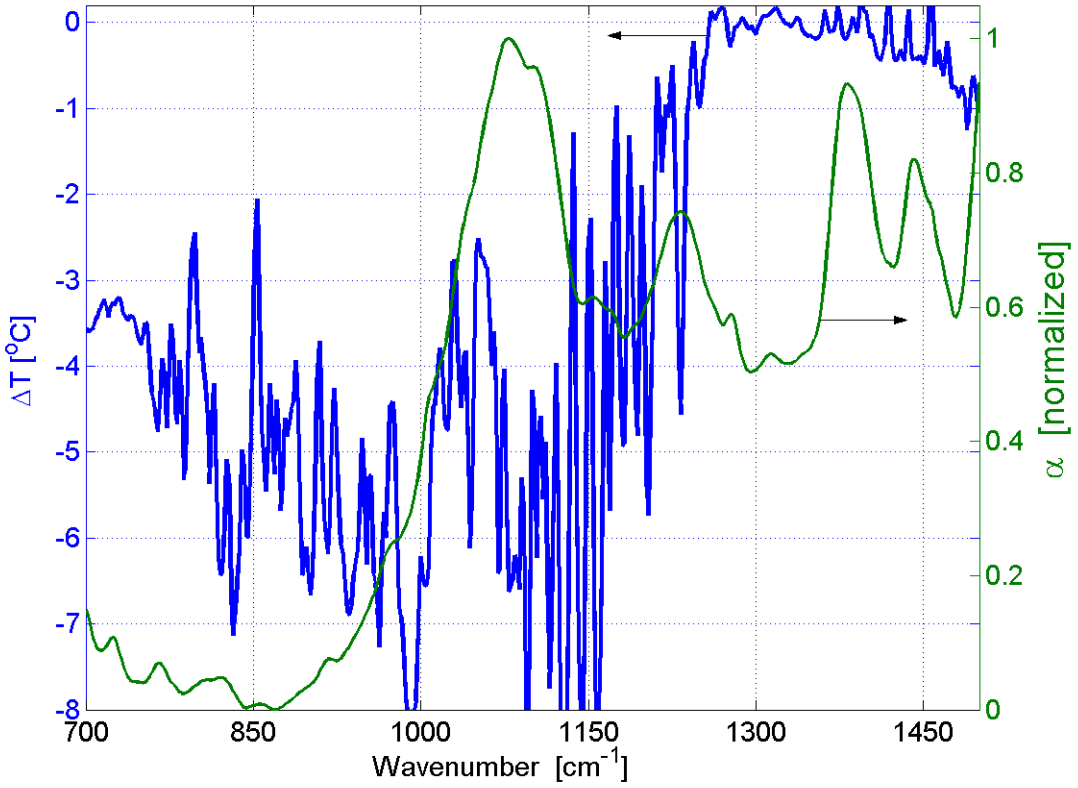

Fig. 7 - Spectral brightness temperature difference between the ambient atmosphere and the effective brightness temperature along the LOS. The normalized spectral mass extinction coefficient of the bio-aerosols is also shown.

Measurements were taken continuously for 6 minutes (2150 measurements at 5.5 Hz). The bio-aerosols were continuously injected with the dust blower for 4 minutes ; starting at measurement number ~200 and stopped at measurement number ~1500. In Fig. 8 we show the result of the identification algorithm where we estimated the mass extinction spectrum $\hat{\alpha}(\lambda)$. For Background measurements we used measurements that were taken 20 minutes prior to the experiment. The correlation coefficient *r* between the estimated mass extinction spectrum $\hat{\alpha}(\lambda)$ and the library spectra $\alpha(\lambda)$ is 0.97 and clearly show a positive identification of the bi-aerosols cloud as BG aerosols.

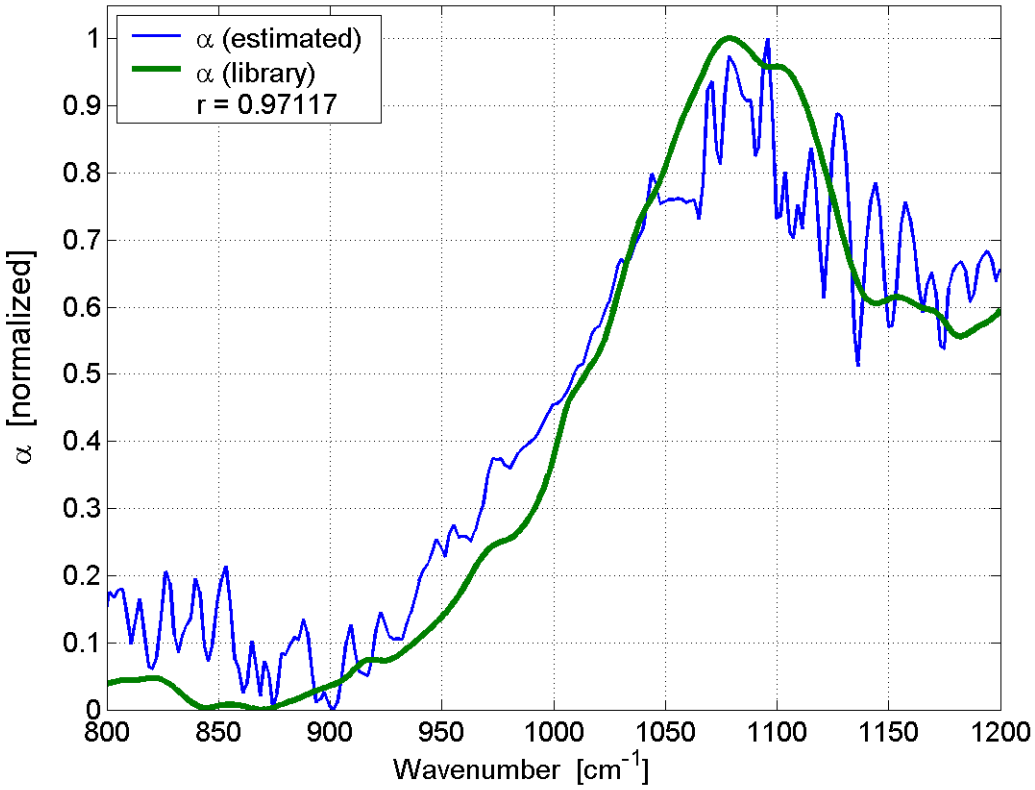

Fig. 8 - Estimated mass-extinction spectrum $\hat{\alpha}(\lambda)$ of the bio-aerosol cloud with the identification algorithm and the library spectra $\alpha(\lambda)$ for BG . The correlation coefficient between the two is 0.97.

In Fig.9 the result of the detection algorithm for the estimated mass-column density $\hat{\rho}(n)$ is shown for the 2150 measurements. A three seconds moving average (i.e., 17 sequential measurements) process was preformed on the estimated $\hat{\rho}(n)$ to reduce noise. A detection threshold γ computed with the EM model is superimposed in the figure. The threshold of detection indicates the appearance of the cloud at measurement number 220 and the disappearance of the cloud at measurement number 1460 - both in a good agreement with the recorded time-sequence of the experiment. The negative concentration in the figure is the result of using background measurements that were taken 20 minutes prior to the experiment and are do not approximate the background condition during the experiment. The difference in Fig. 9 for measurements 1-200 and 1600-2150 clearly show that the background condition did change during the 6 minutes experiment. In Fig. 9a we show the result of the detection algorithm for the estimated mass-column density $\hat{\rho}(n)$ when the first 150 measurements (1-150) were used as background (the BG release started at measurement number ~200).

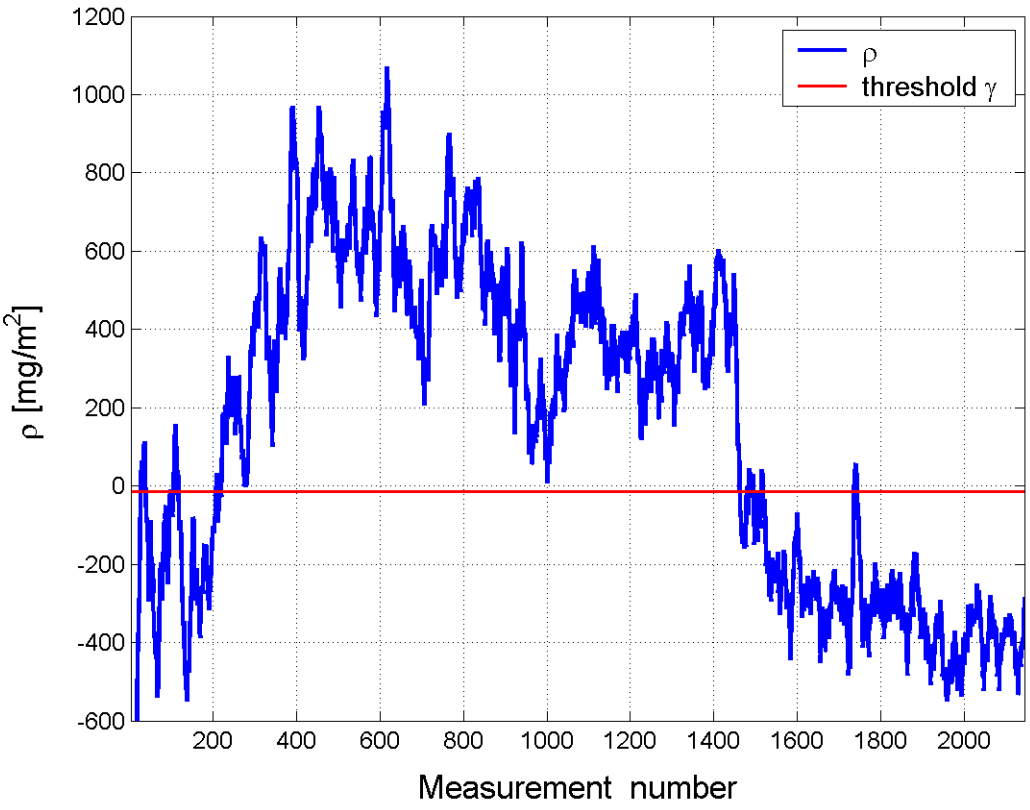

Fig. 9 - Estimated mass-column density $\hat{\rho}(n)$ for BG during the 2150 measurements and a detection threshold γ. A three seconds moving average (i.e., 17 sequential measurements) process was preformed on the estimated $\hat{\rho}(n)$ to reduce noise. Background measurements were taken 20 minutes prior to the experiment.

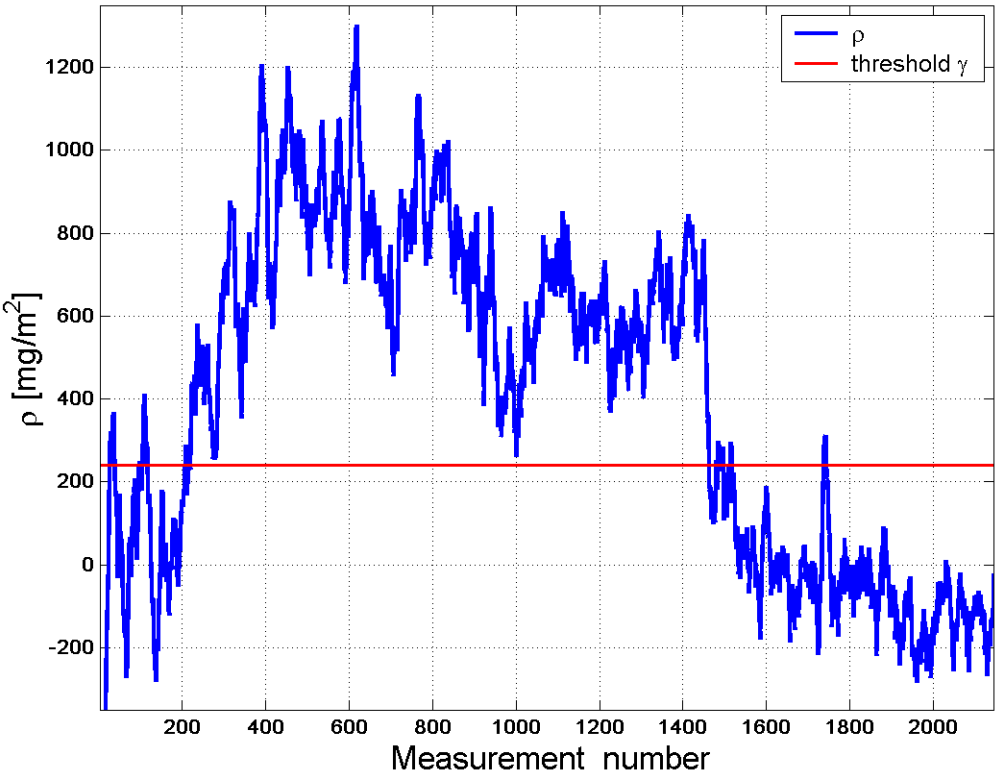

Fig. 9a – same as Fig. 9 but for background we used the first 150 measurements of the experiment.

The pdf (computed with the EM algorithm) for $\hat{\rho}(n)$ of Fig. 9 is shown in Fig. 10 with the histogram of $\hat{\rho}(n)$. The threshold $\gamma = -14.87\ mg\ m^{-2}$ is the location of the intersection of $pdf(\hat{\rho} \mid H_0)$ and $pdf(\hat{\rho} \mid H_1)$. The probability of detection is $P_D(\gamma) = 0.98$ and the probability of false alarm is $P_{FA}(\gamma) = 0.02$. These probabilities are for three seconds of averaging process (Fig. 9).

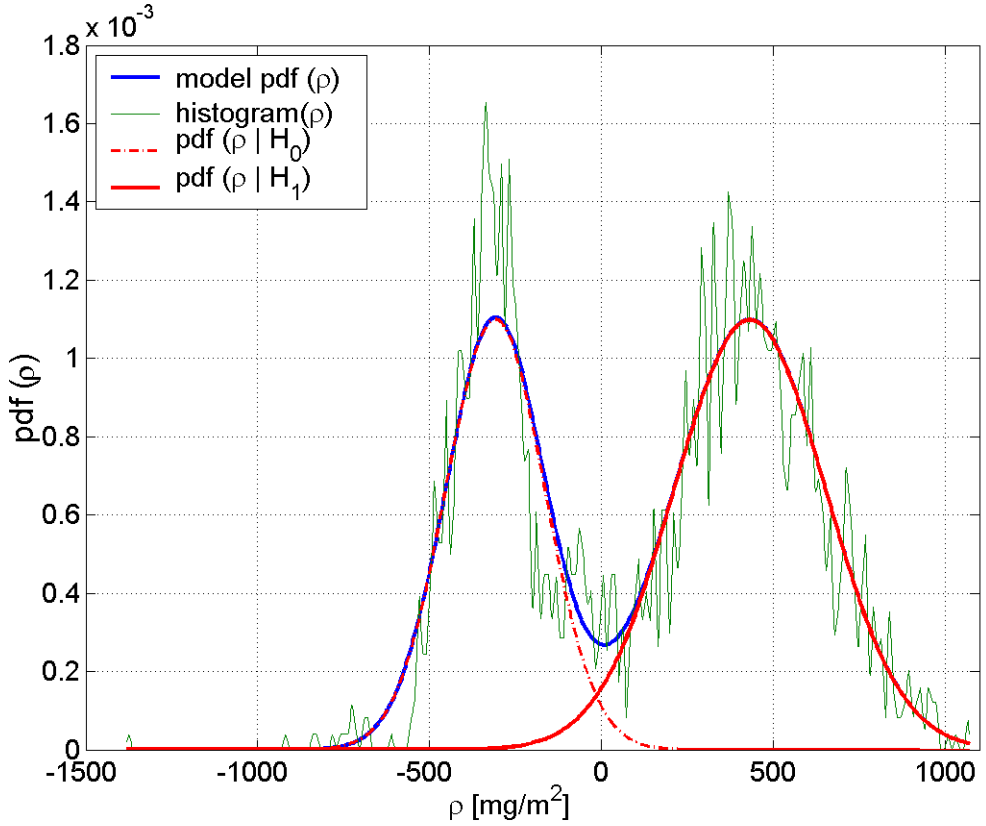

Fig. 10 – The pdf model for $\hat{\rho}(n)$ (Fig. 9a) computed with the EM algorithm, the data $\hat{\rho}(n)$ histogram and the two pdf for the two hypothesis H_0 and H_1.

In Fig. 11 we show the detector score $s(n)$ computed with the matched filter anomaly algorithm, where a three seconds moving average process was used on the scores. The threshold of detection indicates the appearance of the cloud at measurement number 215 and the disappearance of the cloud at measurement number 1513 which is again in a good agreement with the time-sequence of the experiment. The histogram of the scores and the pdf for the model along with the pdfs for the two hypotheses H_0 and H_1 are shown in Fig. 12.

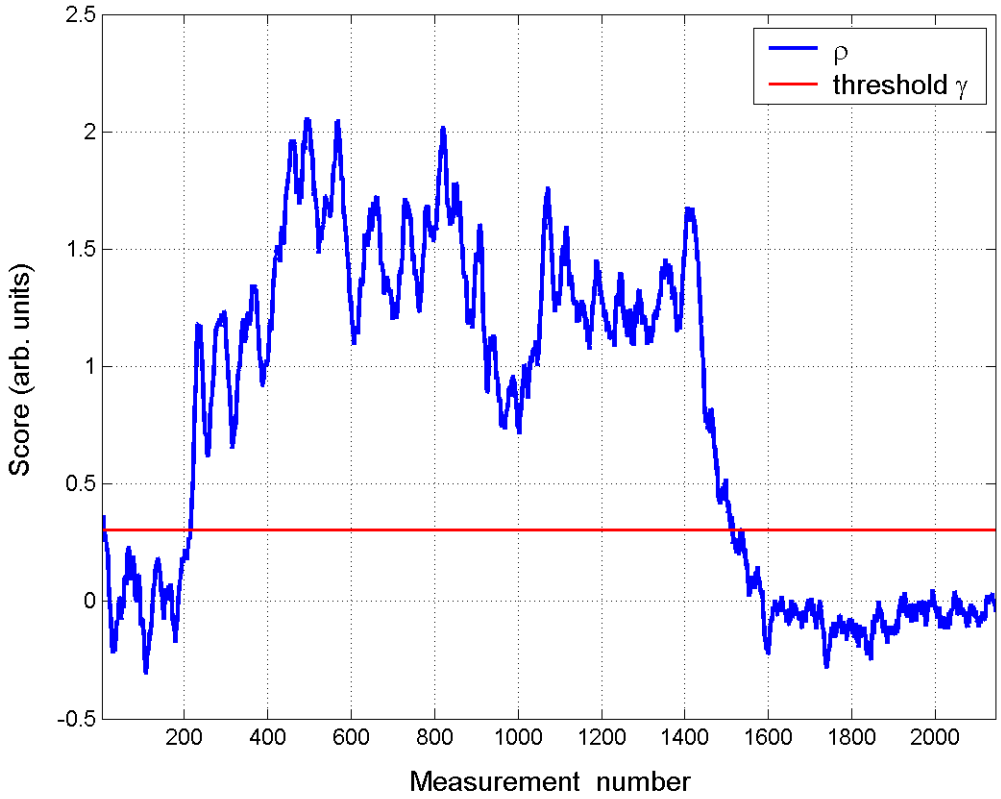

Fig. 11 - Matched filter score $s(n)$ for BG cloud during the 2150 measurements and a detection threshold γ. A three seconds moving average (i.e., 17 sequential measurements) process was preformed on the estimated $s(n)$ to reduce noise.

The threshold for the pdf model is $\gamma = 0.303$. The probability (for a three seconds of averaging) of detection is $P_D(\gamma) = 0.996$ and the probability of false alarm is $P_{FA}(\gamma) = 0.0016$. The shape of the score $s(n)$ is similar to the shape of the estimated $\hat{\rho}(n)$ in Fig. 9, but with a better signal-to-noise ratio (SNR). The reduction of SNR is the "cost" of the estimation process over the "simple" anomaly detection process. The improved SNR is also reflected in improved probability of detection ; 0.98 for Fig. 9 and 0.996 for Fig. 11.

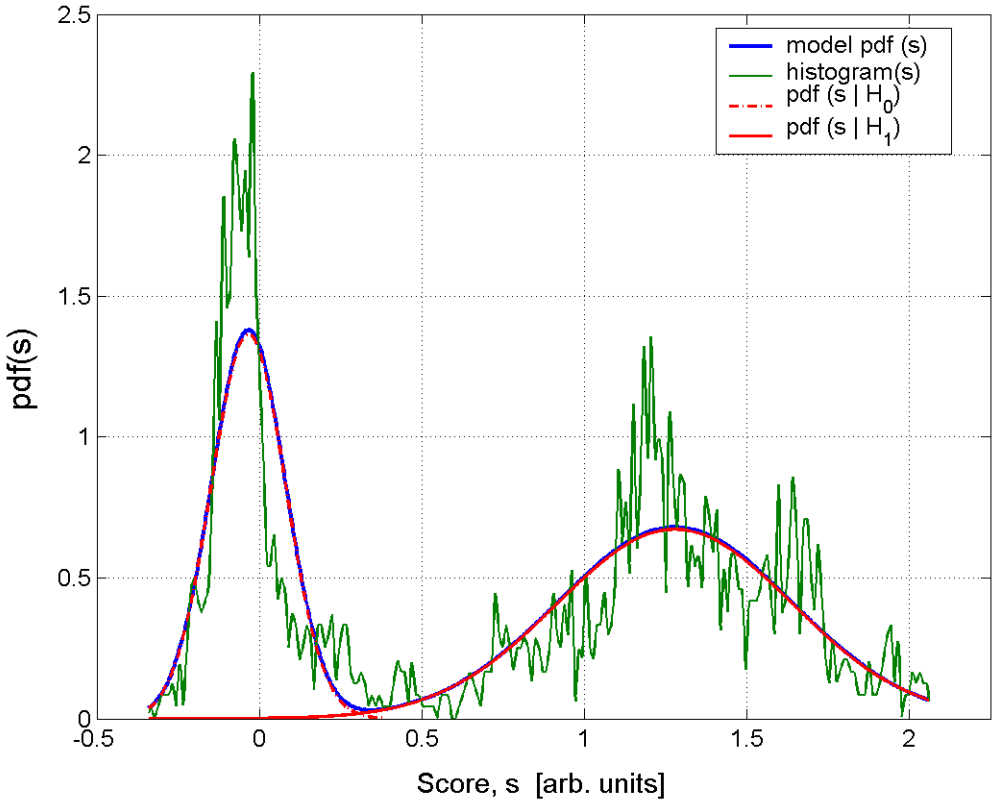

Fig. 12 – same as Fig. 10 but for the matched filter score s of Fig. 11.

2. OPEN-AIR RELEASE OF KAOLIN DUST

A thick cloud of Kaolin dust with uneven density was generated in the open chamber. The total amount of Kaolin used in the experiment is not known. An estimate of the spectral brightness temperature difference between the ambient atmospheric temperature and the effective brightness temperature along the LOS is less than 5 degrees (Fig. 7).

In Fig 13. we show the Mass extinction coefficient of Kaolin material.

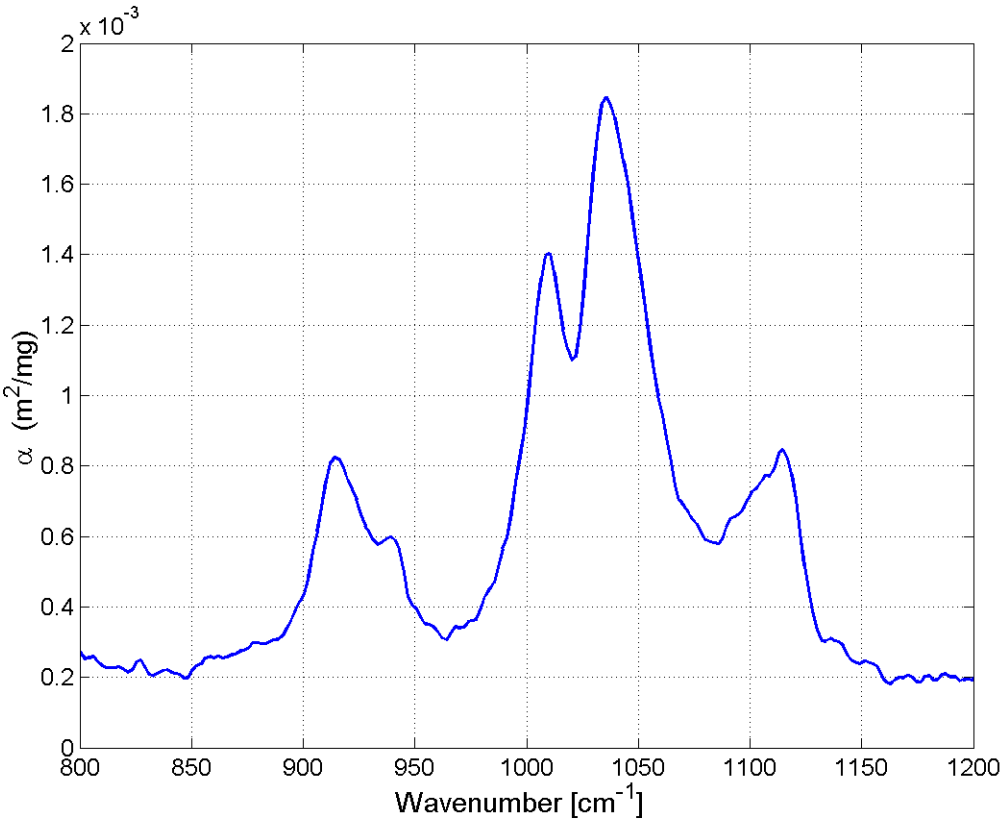

Fig. 13 – Mass extinction coefficient of Kaolin material.

The figure shows that the extinction value for Kaolin is about two orders of magnitude higher than for BG. Non-linearity in the transmission $e^{-\alpha(\lambda)\rho}$ will appear for mass-column density $\rho > 100\ mg\ m^{-2}$ for which the optical depth is greater than 0.2.

In Fig. 14 we show the result of the identification algorithm where we estimated the mass extinction spectrum $\hat{\alpha}(\lambda)$. The correlation coefficient *r* between the estimated mass extinction spectrum $\hat{\alpha}(\lambda)$ and the library spectrum $\alpha(\lambda)$ is 0.82. The relative magnitude in the deduced spectrum is distorted and also there is a slight shift in the peak locations. The issue of non-linearity due to the large optical depth may provide a partial explanation for this. This issue will be revisited in the future. Nevertheless, it is easy to see the similarity between the two spectra which indicate a positive identification of the aerosol cloud as Kaolin.

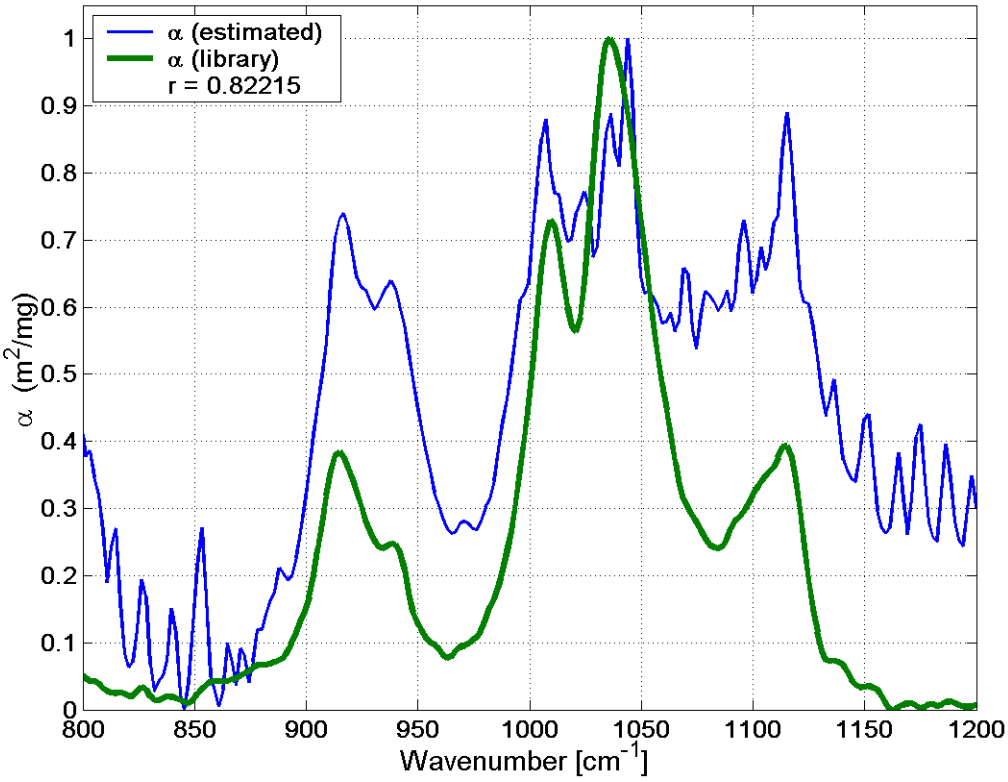

Fig. 14 - Estimated mass-extinction spectrum $\hat{\alpha}(\lambda)$ of the aerosol cloud with the identification algorithm and the library spectra $\alpha(\lambda)$ of Kaolin The correlation coefficient between the two is 0.82.

In Fig.15 the result of the detection algorithm for the estimated mass-column density $\hat{\rho}(n)$ is shown. A three seconds moving average (i.e., 17 sequential measurements) process was preformed on the estimated $\hat{\rho}(n)$ to reduce noise. The first 300 measurements are pre-release measurements. The threshold for the pdf model is $\gamma = 23.7\ mg\ m^{-2}$. The probability of detection is $P_D(\gamma) = 0.991$ and the probability of false alarm is $P_{FA}(\gamma) = 0.001$.

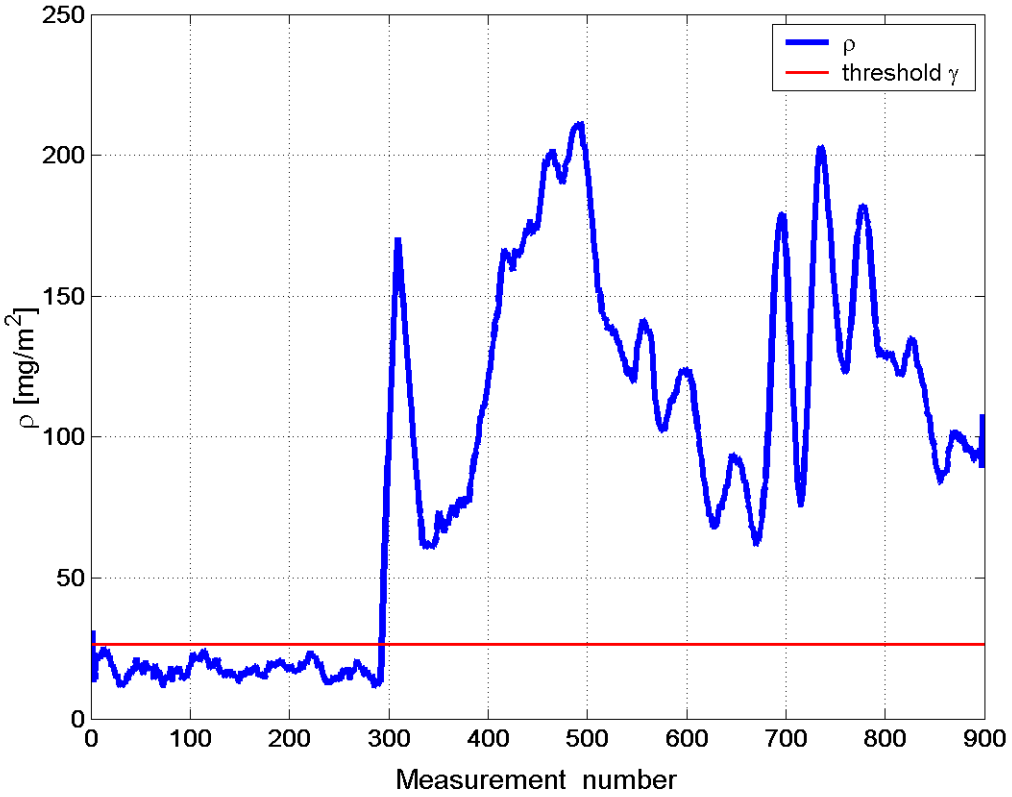

Fig. 15 - Estimated mass-column density $\hat{\rho}(n)$ for Kaolin cloud and a detection threshold γ. A three seconds moving average (i.e., 17 sequential measurements) process was preformed on the estimated $\hat{\rho}(n)$ to reduce noise.

In Fig. 16 we show the detector score $s(n)$ computed with the matched filter anomaly algorithm, where a three seconds moving average process was used on the scores. The threshold for the pdf model is $\gamma = 5.5 \cdot 10^{-17}$. The probability of detection is $P_D(\gamma) = 0.995$ and the probability of false alarm is $P_{FA}(\gamma) = 0.0026$. Again we see that the "cost" of estimation (Fig. 14) is to lower probability of detection (0.991).

Figs. 15 and 16 show that both algorithm detected the onset of the cloud. The end of the presence of the cloud within the FOV is found at measurement 856 with the matched filter algorithm and was not found with the first detection algorithm (mass-column density estimation) due to the fact that the required SNR to estimate mass-column density is higher than that for a matched filter. Unfortunately only about 50 measurements were collected after the end of the release and we needed to average 17 sequential measurements to reduce measurements noise. Thus, not enough measurements were available after the end of the release and the end of the release is not identified well in Fig. 15.

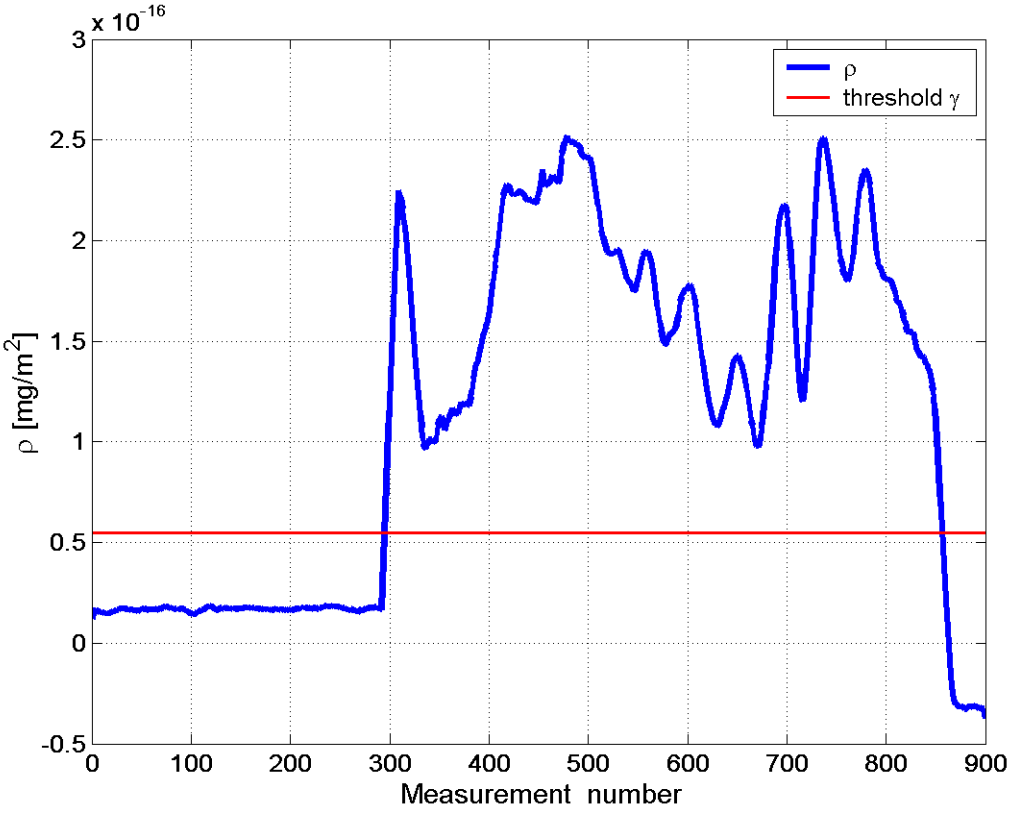

Fig. 16 - Matched filter score $s(n)$ for Kaolin cloud and a detection threshold γ. A three seconds moving average (i.e., 17 sequential measurements) process was preformed on the estimated $s(n)$ to reduce noise.

SUMMARY

A simple radiative transfer model was developed to address the problem of identification detection and estimation of aerosol cloud with FTIR sensor along a horizontal LOS. We separate the sensor measurements into two parts; signal-information that is affected by the presence of the cloud via its transmission $e^{-\alpha(\lambda)\rho}$ and a second part that is not affected by the presence of the cloud and can be viewed as a large offset.

Advanced hyperspectral identification, detection and estimation algorithms, based on radiative transfer theory and statistical signal processing methods (expectation maximization, maximum likelihood, matched filters and orthogonal projection) were developed. We show the performance of our algorithms where a high sensitivity FTIR sensor (HISPEC) was used in two experiments (at Dugway Proving Ground, Utah) to measure open-air release of (1) dry BG aerosol cloud and (2) Kaolin dust cloud. The temperature difference (background to ambient air) was small ($< 5\ ^{o}K$) in the two experiments.

The identification algorithm identifies the BG material beyond any doubt as can be seen in Fig. 8. The detection of the presence (and absence) of the BG cloud was excellent and the estimation of its mass-column density is reasonable but cannot be verified. Measurements were taken continuously at a distance of 50 meters through a horizontal line of sight with a complex background (sky and mountains at a distance of a few tens of kilometers). A probability model and a threshold for detection were computed for the BG mass-column density estimation (Fig.

9). The probability of detection is 0.98 and the probability of false alarm is 0.02. These probabilities are for three seconds of averaging process. The probability of detection computed for anomaly detection with a matched filter algorithm (Fig. 11) is slightly higher (0.996) and reflect the "cost" involved in the estimation process.

The identification of the Kaolin dust is less good (correlation coefficient value of 0.82) than the identification of the BG (correlation coefficient value of 0.97) but does show a high level of identification as can be seen in Fig. 14. We think that the presence of optically thick cloud (non-linearity in its transmission) is partially to account for the distortion of the absorption peak values and their precise location. We intend to explore this issue in the future. The detection of the presence of the Kaolin cloud was good and the estimation of its mass-column density is reasonable but cannot be verified. A probability model and a threshold for detection were computed for the Kaolin mass-column density estimation (Fig. 15). The probability of detection is 0.991 and the probability of false alarm is 0.001. These probabilities are for three seconds of averaging process.

Our experiment and analysis clearly show the feasibility of passive remote sensor to detect and identify BG particles. These results are encouraging and more experiments to validate our models and to explore their limitations are planned.

ACKNOWLEDGEMENTS

I thank Thomas Gruber (MESH) for his help during the experiments. A. Ben-David was supported by the U.S. Army Soldier and Biological Chemical Command, Edgewood Chemical Biological Center under Contract No. DAAM01-94-C-0079

REFERENCES

1. Berk, A., G. P. Anderson, L. S. Bernstein, P. K. Acharya, H. Dothe, M. W. Matthew, S. M. Adler-Golden, J. H. Chetwynd, Jr., S. C. Richtsmeier, B. Pukall, C. L. Allred, L. S., Jeong and M. L. Hoke, "MODTRAN4 radiative transfer modeling for atmospheric correction", *proc. of SPIE Optical spectroscopic techniques and instrumentation for atmospheric and space research III*, 19-21 July 1999, Vol. 3756, 348-353 (1999).

2. Schildkraut, E. R., R. Connors and A. Ben-David, "Initial test results from ultra-high sensitivity passive FTIR instrumentation (HISPEC)", Proceedings of the International Symposium on Spectral Sensing Research, 10-15 June, Quebec City Canada, pp. 365-374, Science and Technology Corp. Hampton, VA (2001).

3. Ben-David A., and A. Ifarraguerri, "Computation of a spectrum from a single-beam Fourier-transform infrared interferogram" Appl. Opt. **41**, 1181-1189 (2002).